Title	Real space mapping of polarization dynamics and hysteresis loop formation in relaxor-ferroelectric PbMg1/3Nb2/3O3-PbTiO3 solid solutions
Authors(s)	Rodriguez, Brian J., Jesse, S., Morozovska, A. N., et al.
Publication date	2010-08
Publication information	Rodriguez, Brian J., S. Jesse, A. N. Morozovska, and et al. “Real Space Mapping of Polarization Dynamics and Hysteresis Loop Formation in Relaxor-Ferroelectric PbMg1/3Nb2/3O3-PbTiO3 Solid Solutions.” AIP, August 2010. https://doi.org/10.1063/1.3474961.
Publisher	AIP
Item record/more information	http://hdl.handle.net/10197/5172
Publisher's statement	The following article appeared in Journal of Applied Physics, 108, 042006 (2010) and may be found at http://link.aip.org/link/doi/10.1063/1.3474961. The article may be downloaded for personal use only. Any other use requires prior permission of the author and the American Institute of Physics.
Publisher's version (DOI)	10.1063/1.3474961

JOURNAL OF APPLIED PHYSICS **108**, 042006 (2010)

Real space mapping of polarization dynamics and hysteresis loop formation in relaxor-ferroelectric $PbMg_{1/3}Nb_{2/3}O_3-PbTiO_3$ solid solutions

B. J. Rodriguez,[1] S. Jesse,[2] A. N. Morozovska,[3] S. V. Svechnikov,[3] D. A. Kiselev,[4] A. L. Kholkin,[4] A. A. Bokov,[5] Z.-G. Ye,[5] and S. V. Kalinin[2,a)]
[1]*University College Dublin, Belfield, Dublin 4, Ireland*
[2]*Oak Ridge National Laboratory, Oak Ridge, Tennessee 37831, USA*
[3]*V. Lashkaryov Institute of Semiconductor Physics, National Academy of Science of Ukraine, 41, Prospect Nauki, 03028 Kiev, Ukraine*
[4]*Department of Ceramics and Glass Engineering and CICECO, University of Aveiro3810-193 Aveiro, Portugal*
[5]*Department of Chemistry and 4D LABS, Simon Fraser University, Burnaby, British Columbia, V5A 1S6, Canada*

(Received 11 October 2009; accepted 5 May 2010; published online 31 August 2010)

Polarization switching in ergodic relaxor and ferroelectric phases in the $PbMg_{1/3}Nb_{2/3}O_3-PbTiO_3$ (PMN-PT) system is studied using piezoresponse force microscopy, single point electromechanical relaxation measurements, and voltage spectroscopy mapping. The dependence of relaxation behavior on voltage pulse amplitude and time is found to follow a universal logarithmic behavior with a nearly constant slope. This behavior is indicative of the progressive population of slow relaxation states, as opposed to a linear relaxation in the presence of a broad relaxation time distribution. The role of relaxation behavior, ferroelectric nonlinearity, and the spatial inhomogeneity of the tip field on hysteresis loop behavior is analyzed in detail. The hysteresis loops for ergodic PMN-10%PT are shown to be kinetically limited, while in PMN with larger PT content, true ferroelectric hysteresis loops with low nucleation biases are observed. © *2010 American Institute of Physics*. [doi:10.1063/1.3474961]

I. INTRODUCTION

The unique electromechanical and dielectric properties of relaxor ferroelectrics resulting from the existence of temperature-dependent polar nanostructures and diffuse phase transitions enable numerous industrial applications.[1] At high temperatures, relaxors and ferroelectrics exist in a nonpolar paraelectric state, but unlike ferroelectrics which transform to a ferroelectric phase below the Curie temperature (T_C), relaxors undergo a transition to a relaxor state at the Burns temperature (T_B) near which dynamic polar nanodomains or nanoregions (PNRs) with random dipole moment directions appear.[2] As the temperature is decreased, the PNRs become less responsive until they are frozen and the relaxor undergoes a transition into a nonergodic state which lacks long range ferroelectric order and bears a resemblance to the dipolar glass state. Compositional disorder is a characteristic of all relaxors. Below and hundreds of degrees above T_B, compositional order is fixed, and is always inhomogeous (small regions of order are surrounded by a disordered matrix).[2]

The unique properties of relaxor ferroelectrics have raised fundamental interest in understanding the mesoscopic structures in these materials, including microdomain and nanodomain populations, polarization distributions, and their evolution with external electric field and temperature. This interest prompted a number of studies on relaxors using atomic force microscopy (AFM) (Ref. 3) and, later on, piezoresponse force microscopy (PFM).[4] Abplanalp *et al.*[5] observed diffuse domains with irregular 180°-domain walls and domain structure that resembled a fingerprint pattern in an unpoled $Pb(Zn_{1/2}Nb_{2/3})O_3-8\%PT$ single crystal using both out-of-plane (vertical) and in-plane (lateral) PFM measurements. Ferroelastic domains were also observed and the switching of antiparallel domains was demonstrated with the application of +/−30 V.[5] Similar domain patterns were revealed in relaxor $PbMg_{1/3}Nb_{2/3}O_3-10\%PbTiO_3$ (PMN-10%PT) single crystals by Vakhrushev *et al.*[6] and, later on, by Bai *et al.*[7] In subsequent studies, Shvartsman and Kholkin[8] and Salak *et al.*[9] measured the temperature dependence of the electromechanical response in PMN-20%PT single crystals and in $BaTiO_3$ ceramics doped with $La(Mg_{1/2}Ti_{1/2})O_3$, respectively. In PMN-20%PT, ferroelectric domains were found to contain PNRs that existed above T_C. Similarly, in doped $BaTiO_3$, the electromechanical response due to ferroelectric domains disappeared above T_C, while small residual domains could still be observed. Interestingly, even above the transition temperature, local hysteresis loops could still be measured. The observed nanoscale behavior was found to correlate with macroscopic studies.[9] Vertical and lateral PFM imaging has also been employed to measure the domain structure in PMN-30%PT crystals[10] and in relaxor lead lanthanum zirconate-titanate ceramics (PLZT).[11] The complex domain structure observed in relaxor PLZT (La content 9.75%) was attributed to La-induced disorder and a correlation length of ∼50 nm was determined from the autocorrelation of the PFM images. Recently, Shvartsman and Kholkin[12] observed nanodomains well above the structural phase transition by PFM, and attributed this

---

[a)]Electronic mail: sergei2@ornl.gov.

behavior to a transient relaxor-ferroelectric state near the surface of the crystal. In principle, PNRs should exist in relaxors below T_B($\sim$650 K) but their direct study is hampered by their small size ($\sim$0.5–5 nm) and apparent dynamic character.

The large number of studies of domain structures in relaxors as a function of composition and temperature is belied by the lack of detailed studies of local switching behavior and hysteresis loop formation mechanisms. In conventional ferroelectrics, tip-induced switching in PFM is a first order process and domain nucleation requires a finite bias below the tip.[13] The relaxation (decay) of a bias-induced domain proceeds through the sidewise and vertical motion of the domain wall. In relaxors, the mechanism of local bias-induced phenomena is apparently different and depends largely on the nature of the tip-bias induced phase and its interaction with defects and the relation between the effective diameter of the tip and the scale of characteristic inhomogeneity in the material. The local bias-induced phenomena in relaxors include the existence of apparent hysteresis far *above* the nominal T_C (arising due to tip-mediated ferroelectric phases), activationless local switching due to pre-existing polarization states, the existence of surface phases, etc.[14]

Here, we explore the dynamic aspects of disorder in relaxors and gain an understanding of local phase stability and evolution under an electric field by studying the static domain structures and domain dynamics as a function of composition by PFM and switching spectroscopy PFM (SS-PFM).

II. EXPERIMENTAL DETAILS

A. Materials

As a model system, we have chosen several members of the $(1-x)\mathrm{Pb}(\mathrm{Mg}_{1/3}\mathrm{Nb}_{2/3})\mathrm{O}_3-x\mathrm{PbTiO}_3$ family, including relaxor PMN-10%PT and ferroelectric PMN-32%PT and PMN-35%PT, the latter having a composition close to the morphotropic phase boundary. PMN-10%PT is a relaxor with a small rhombohedral distortion below $T_C=275$ K.[15] The dielectric maximum occurs at $T_{\max}=300$ K (at 1 kHz). PMN-32%PT and PMN-35%PT already exhibit a long-range ferroelectric order at room temperature described by the monoclinic *Pm* phase.[16,17] In all three samples, T_B is about 650 K. The (001) crystal surfaces were mirror-polished using a series of diamond pastes for PFM examination and supplied with counter electrodes (silver paint).

B. PFM imaging and spectroscopy

PFM imaging and time- and voltage spectroscopy were performed using a commercial AFM (Veeco Multimode) equipped with both Nanoscope IIIA and flexible digital controller from Nanonis Gmbh. Home-built data acquisition electronics (National Instruments PXI platform) were used for collecting the data. Relaxation and switching spectroscopy measurements are performed using MATLAB/LABVIEW acquisition and analysis software.[18] A custom-built, shielded sample holder was used to directly bias the tip and to avoid capacitive cross-talk. Measurements were performed using Au–Cr coated Si tips (Micromasch, spring constants $k\sim 6$, 40 N/m).

In PFM, the conducting AFM tip is brought into contact with the surface, and the local piezoelectric response is detected as the first harmonic component, $A_{1\omega}$, of the tip deflection, $A=A_0+A_{1\omega}\cos(\omega t+\varphi)$, during application of the periodic bias, $V_{\mathrm{tip}}=V_{\mathrm{dc}}+V_{\mathrm{ac}}\cos(\omega t)$, to the tip. The phase of the electromechanical response of the surface, φ, yields information on the polarization direction below the tip. For c^- domains (polarization vector oriented normal to the surface and pointing downward), the application of a positive tip bias results in the expansion of the sample, and surface oscillations are in phase with the tip voltage, $\varphi\approx 0$. For c^+ domains, $\varphi\approx 180°$. The piezoresponse amplitude, $A=A_{1\omega}/V_{\mathrm{ac}}$, defines the local electromechanical activity. PFM images can be conveniently represented as the 'mixed' signal, $A_{1\omega}\cos(\varphi)/V_{\mathrm{ac}}$, where $A_{1\omega}$ is the amplitude of the first harmonic of the measured response, provided that the phase signal varies by $\approx 180°$ between domains of opposite polarities.

In relaxation measurements, dc bias pulses of specified magnitude and duration are applied to the conducting AFM tip in contact with the sample, and the resulting electromechanical response is measured as a function of time for a specified duration.[19] The response is measured in both the ON and OFF states, and the curves can be averaged for multiple pulses. The resulting relaxation curves can be fitted to a given functional form, and relaxation parameters can be determined for a single point. In the spectroscopic imaging mode, the measurements are performed over a two-dimensional (2D) grid of points and fitting parameters are plotted as 2D maps.[20,21] The detailed studies of local relaxation behavior at the surfaces of PMN-PT crystals are reported elsewhere.[22]

In piezoresponse force spectroscopy (PFS), the dc bias applied to the tip is varied to follow a triangular wave, and the nucleation and growth of the ferroelectric domain below the tip are reflected in the change of the effective electromechanical response. The resulting hysteresis loops contain information on ferroelectric switching at a single location. Spatial variability of switching behavior is probed by SS-PFM, in which hysteresis loops are acquired at each point of a user-specified grid. To conduct SS-PFM measurements, the tip approaches the surface vertically until a specified contact force is achieved (usually $\sim$500 nN), remains at that location during the acquisition of the hysteresis loop, and is then retracted and moved to the next location in a predefined square-grid. Individual hysteresis loops in the resulting three-dimensional data set are analyzed to extract parameters characterizing local switching behavior which are then plotted as 2D spatially resolved maps. Detailed studies of local switching behavior at the surfaces of PMN-10%PT crystals are reported elsewhere.[23]

III. RESULTS AND DISCUSSION

A. Static domain PFM imaging

Topography and domain structure for the three chosen PMN-PT compositions (PMN-10%PT, PMN-32%PT, and

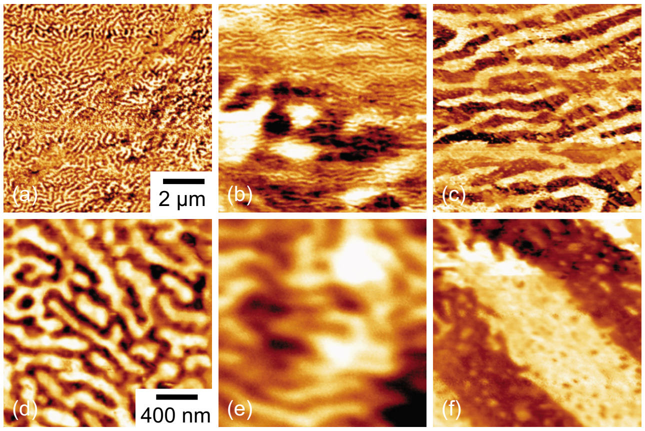

FIG. 1. (Color online) Domain structures (mixed VPFM images at two scan sizes) in PMN–xPT as a function of composition for (a, d) 10%PT, (b, e) 32%PT, and (c, f) 35%PT.

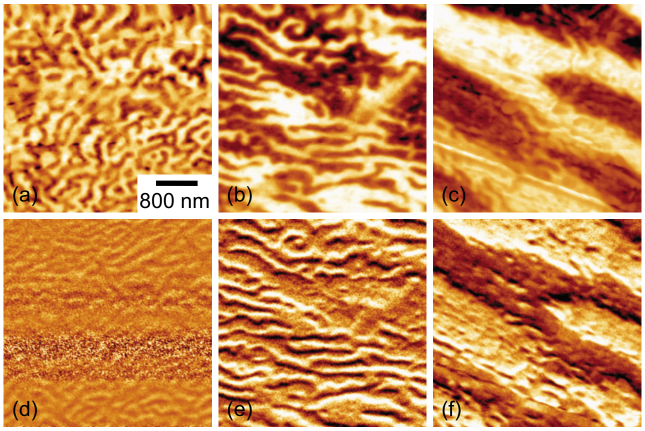

FIG. 2. (Color online) VPFM and LPFM in PMN–xPT as a function of composition. (a)–(c) Mixed VPFM and (d)–(f) mixed LPFM for (a, d) 10%PT, (b, e) 32%PT, and (c, f) 35%PT. VPFM and LPFM data were measured sequentially and have not been corrected for possible tip-drift.

PMN-35%PT) are shown in Fig. 1. The domain structure in PMN-10%PT [Figs. 1(a) and 1(d)] is formed by well-defined labyrinthine domains of 100–200 nm characteristic size. The domain boundaries are generally smooth and the amplitude contrast is nonuniform on the length scale above the characteristic domain size, possibly due to variations in surface topography. Note that the observed domain pattern, highly reminiscent of the labyrinthine domains in ferromagnetic films,[24] is unusual for classical ferroelectrics. This is further reinforced by the fact that at room temperature, PMN-10%PT is well above T_C ($\cong$280 K) and, according to focused x-ray measurements, is in the nominally cubic state in the near-surface regions.[22] The presence of these domains strongly suggests that the symmetry of the surface phase in PMN-10%PT is lower than cubic, *albeit* with very small lattice distortion. While similar domain structures[6] were observed in the ergodic phases of several relaxor systems including also PLZT and $\text{Pb}(\text{Zn}_1/3\text{Nb}_2/3)\text{O}_3$-PT,[11,25,26] their exact origin remains unknown.

In contrast to the labyrinthine structure in PMN-10%PT, where the domain walls can have arbitrary, seemingly uncorrelated directions, PMN-32%PT and PMN-35%PT show banded domain structure [Figs. 1(b) and 1(e) and Figs. 1(c) and 1(f), respectively]. The thickness of the banded domains may vary from ~100 nm (i.e., the same as for labyrinthine domains in PMN-10%PT) to ~1 μm. A number of small (10–50 nm) domain "islands" of opposite polarity within the macroscopic domains are clearly seen (note that such small islands are practically absent in PMN-10%PT). The domain boundaries are strongly roughened and the PFM amplitude changes rapidly at the domain wall. Note that the PFM amplitude is much higher within normal domains than within the labyrinthine pattern of PMN-10%PT. This difference can be related to the fact that at room temperature the PMN-32%PT and PMN-35%PT crystals are both in the monoclinic ferroelectric phase,[27] while PMN-10%PT is in the macroscopically cubic ergodic relaxor phase. Close inspection of amplitude and phase images illustrates that labyrinthine domains are superimposed over macroscopic domains, i.e., the two can coexist in each point for the PMN-32%PT solid solutions.

To gain insight into the behavior of in-plane polarization components, the three compositions were imaged using lateral PFM as well. The comparison of vertical and lateral PFM (VPFM and LPFM, respectively) data is shown in Fig. 2. For all compositions, the LPFM image shows a clearly visible contrast that could be, in principle, interpreted as the presence of an in-plane polarization component. However, in both PMN-32%PT and PMN-35%PT crystals one can observe a clear correspondence between the vertical and lateral domains so that the domain walls in both images coincide. This behavior is consistent with LPFM behavior at 180°-domain walls[28–30] and thus can be ascribed to a cross-coupling with the vertical signal. Based on the examination of the images, we conclude that the in-plane component contribution to the LPFM signal is below the detection limit (less than ~20% of vertical signal). Hence, while in the monoclinic *Pm* phase the spontaneous polarization vector may have 24 different directions none of which are perpendicular to the (001) plane (crystal surface),[31] the observed vertical and lateral PFM images are consistent with *purely* out-of-plane polarization orientation for all compositions. PFM data on PMN-10%PT suggests that the close correspondence between VPFM and LPFM exists only in some areas. However, the small size of the observed domains does not allow identifying their orientation and the pure out-of-plane polarization component should be confirmed in future studies.

B. Relaxation dynamics

The local relaxation behavior of the PMN-10%PT crystal surface is studied using time-resolved piezoresponse spectroscopy.[20–22] An example of single-point measurements on mica, LiNbO_3, and PMN-10%PT are shown in Fig. 3(a). While the electromechanical response on mica is (as expected) essentially zero, the response on LiNbO_3 is generally independent on time. These observations illustrate the absence of instrumental and environmental (e.g., electrocapillary) artifacts that can lead to spurious relaxation behavior after application of a dc bias. In comparison, PMN-10%PT shows clear relaxation of electromechanical response consis-

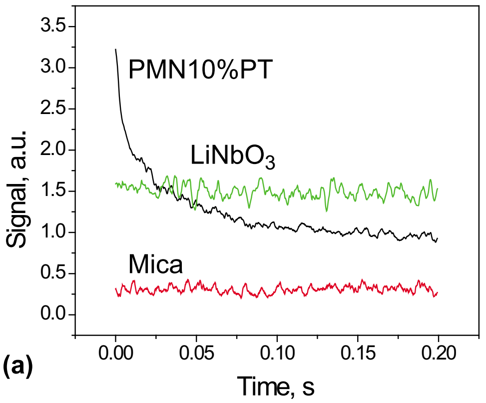

FIG. 3. (Color online) (a) Relaxation curves for PMN-10%PT, $LiNbO_3$, and mica. The observed dynamics suggest that the contribution of possible instrumental and atmospheric artifacts (e.g., electrocapillary effect) to relaxation is minimal. (b) Relaxation curves for PMN-10%PT in bias-on (during the application of 10 V pulse) and bias-off (after bias pulse) states. Several superimposed curves illustrate typical repeatability of experiments. Reproduced with permission from Ref. 40.

tent with a rapid decay of the bias-induced polarization state. The response for bias-on and bias-off states for PMN-10%PT is shown in Fig. 3(b), and illustrates much faster response saturation for the in-field state. The response after poling can be well approximated with a Kohlrausch-Williams-Watts (KWW) stretched exponential dependence $R(t)=R_0-R_1\exp[-(t/\tau_{\mathrm{KWW}})^{\beta}]$ with $\beta<0.5$, or (over shorter time intervals) by a logarithmic time dependence, $R(t)=R_0-R_1\ln t$.[22] Notably, ferroelectric ordering and the growth of favored domains by the application of an external field in ferroelectric relaxors such as PMN-10%PT have been shown to be followed by logarithmically slow relaxation (either as simple logarithm, or its powers) of a uniformly polarized region into randomly oriented nanodomains.[32,33]

To determine the dependence of relaxation behavior on voltage pulse parameters, the measurements were performed as a function of pulse magnitude and length. The results of these bias experiments are shown in Fig. 4(a). For small bias pulses (below 5 V), no relaxation is observed and the electromechanical response is time-independent (suggesting either that the bias-induced polar state did not form, or that it relaxed faster than the experimentally accessible bandwidth). For larger biases, the formation and decay of the bias-induced polar state is clearly observed. Within the noise level of the experiment, the relaxation kinetics follows a logarithmic law [Fig. 4(b)] (which is also consistent with a stretched exponential if the time interval is too short). The data were fitted using $\Delta PR(t)=a_1(V)-b_1(V)\log t$, and the bias dependence of the intercept, $a_1(V)$, and slope, $b_1(V)$, are shown in Figs. 4(c) and 4(d) [$\Delta PR(t)$ represents the piezoresponse signal with subtracted initial background]. Note that the slopes are essentially bias independent while the intercept grows linearly with voltage. The lack of relaxation below 5 V is consistent with either the absence, or a short relaxation time (within the limits of experimental error) of an induced polar state.

The relaxation behavior as a function of pulse length, τ, is shown in Fig. 5. The relaxation behavior is again well-approximated by the logarithmic law, $\Delta PR(t)=a_2(\tau)-b_2(\tau)\log t$. The intercept, $a_2(\tau)$, is initially linear with $\log(\tau)$ and then saturates at several seconds. The slope, $b_2(\tau)$, slightly increases with τ but in general varies by less than a factor of two even while τ changes by three orders of magnitude.

In the first approximation, the relaxation behavior as a function of pulse parameters can be represented by the phenomenological dependence

$$\Delta PR(t)=a(V,\tau)-b(V,\tau)\log t \quad \text{for } t<t_{\mathrm{crit}} \tag{1a}$$

$$\Delta PR=0 \quad \text{for } t>t_{\mathrm{crit}}, \tag{1b}$$

where $\log(t_{\mathrm{crit}})=a(V,\tau)/b(V,\tau)$ is the generalized lifetime of the bias induced polar state. Given that $b_1(V,\tau)\approx b$ does not vary significantly with V and τ, the relaxation kinetics are determined primarily by the amount of switched polarization, i.e., by an offset $a(V,\tau)$. The latter is determined by the pulse bias and duration (before saturation) as

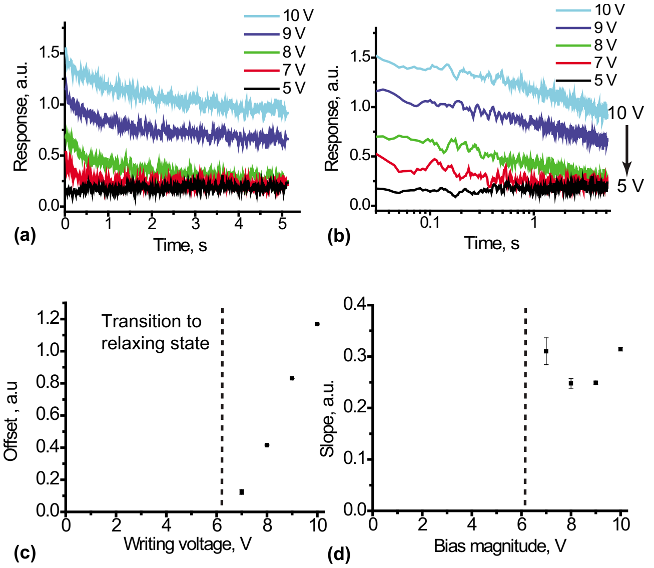

FIG. 4. (Color online) Relaxation behavior in PMN-10%PT after switching off the 30 ms pulses of different magnitude in (a) linear and (b) logarithmic coordinates. Bias dependence of (c) intercept and (d) slope of the relaxation curve in logarithmic coordinates. Vertical dashed line corresponds to the onset of the state with induced polarization.

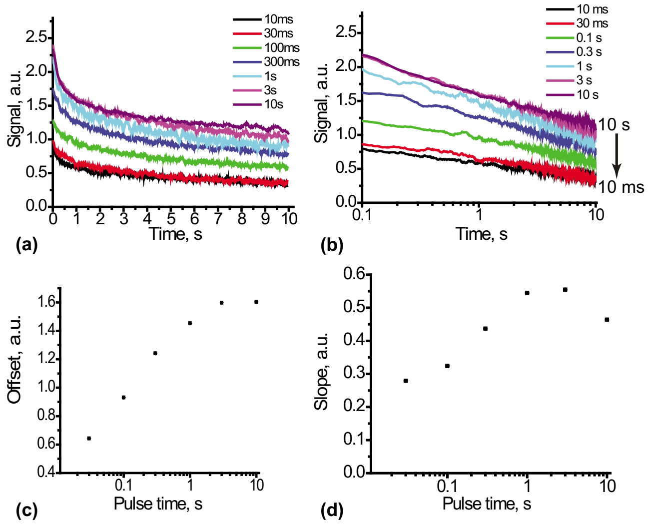

FIG. 5. (Color online) Bias length dependence (for 10 V pulse) of relaxation behavior in PMN-10%PT in (a) linear and (b) logarithmic coordinates. Bias dependence of (c) intercept and (d) slope of the relaxation curve in logarithmic coordinates.

$$a(V,\tau)=(\alpha+\beta\log\tau)f(V), \tag{2}$$

where $f(V)=0$ for $V<V_{\text{crit}}$ and $f(V)=\kappa V$ for $V>V_{\text{crit}}$, and $\beta=\text{constant}$. Note that numerically $\beta\approx b$, suggesting the universality of bias-on (writing) and bias-off (reading) relaxation behavior.

C. Theoretical description of relaxation behavior

The relaxation of the electromechanical response in a PFM experiment is determined by the convolution of three factors, namely, (a) the spatial dispersion due to the nonuniformity of the field produced by the AFM probe, (b) the intrinsic relaxation behavior of the material in a uniform field as a function of the field magnitude and pulse length, and (c) the nonlinear nature of ferroelectric relaxors. The contributions of these factors to observed relaxation behavior are analyzed in detail below.

1. Spatial dispersion in PFM experiment

To analyze the effect of spatial dispersion on the relaxation in a PFM experiment we consider the relaxation of electromechanical response induced by a biased AFM probe for a system with an exponential relaxation (Debye relaxation). Polarization response, p to the inhomogeneous probe electric field was derived from the coupled problem

$$\begin{cases}\Gamma\dfrac{dp}{dt}+\alpha_R p+\beta p^3-\xi\left(\dfrac{1}{\rho}\dfrac{\partial p}{\partial\rho}+\dfrac{\partial^2 p}{\partial\rho^2}+\dfrac{\partial^2 p}{\partial z^2}\right)=-\dfrac{\partial\varphi}{\partial z},\\[2ex] \varepsilon_{33}^{b}\dfrac{\partial^2\varphi}{\partial z^2}+\varepsilon_{11}\left(\dfrac{1}{\rho}\dfrac{\partial\varphi}{\partial\rho}+\dfrac{\partial^2\varphi}{\partial\rho^2}\right)=\dfrac{1}{\varepsilon_0}\dfrac{\partial p}{\partial z},\end{cases} \tag{3}$$

with boundary conditions $\varphi(\rho,z=0)=V_e(\rho,t)$, $\varphi(x,y,z\to\infty)=0$, and initial conditions $p(\mathbf{r},t\le 0)=0$, $\partial p/\partial z|_{z=0}=0$. Here, we introduce the dielectric permittivity of the background[34] or reference[35] state as ε_{33}^{b} (typically $\varepsilon_{33}^{b}\le 10$) and ε_0 is the dielectric constant of vacuum. The potential distribution produced by the AFM probe on the surface of a semi-infinite sample can be approximated as $V_e(\rho,t)=V_a(t)d/\sqrt{\rho^2+d^2}$, where $V_a(t)$ is the applied bias amplitude, d is the effective distance determined by the probe geometry (see Ref. 36), and $\rho=\sqrt{x^2+y^2}$ is the radial coordinate. The potential is normalized assuming the condition of perfect electrical contact with the surface, $V_e(0,t)\approx V_a(t)$. For a flattened tip represented by a disk of radius R_0 in contact with the sample surface, $d=2R_0/\pi$.

Equations (3) linearized with respect to the small deviation of polarization, p, can be rewritten as

$$\Gamma\frac{dp}{dt}+\alpha_R p-\xi\left(\frac{\partial^2 p}{\partial x^2}+\frac{\partial^2 p}{\partial y^2}+\frac{\partial^2 p}{\partial z^2}\right)=E_3^{e}+E_3^{d}(p). \tag{4}$$

The Fourier–Laplace representation on transverse coordinates $\{x,y\}$ and time t of electric field normal component is

$$\tilde{E}_3^{e}(\mathbf{k},z,f)=\tilde{V}_e(\mathbf{k},f)\frac{\cosh(k(h-z)/\gamma_b)}{\sinh(kh/\gamma_b)}\frac{k}{\gamma_b},\qquad \tilde{V}_e(\mathbf{k},f)=V_a(f)\frac{d}{k}\exp(-kd), \tag{5a}$$

$$\tilde{E}_3^{d}(p,\mathbf{k},z,f)=\left(\int_0^z dz'\frac{\tilde{p}(\mathbf{k},z',f)}{\varepsilon_0\varepsilon_{33}^{b}}\cosh\left(k\frac{z'}{\gamma_b}\right)\frac{\cosh(k(h-z)/\gamma_b)}{\sinh(kh/\gamma_b)}\frac{k}{\gamma_b}+\int_z^h dz'\frac{\tilde{p}(\mathbf{k},z',f)}{\varepsilon_0\varepsilon_{33}^{b}}\cosh\left(k\frac{h-z'}{\gamma_b}\right)\frac{\cosh(kz/\gamma_b)}{\sinh(kh/\gamma_b)}\frac{k}{\gamma_b}\right.$$
$$\left.-\frac{\tilde{p}(\mathbf{k},z,f)}{\varepsilon_0\varepsilon_{33}^{b}}\right). \tag{5b}$$

Here, $\gamma_b=\sqrt{\varepsilon_{33}^{b}/\varepsilon_{11}}$ is the "bare" dielectric anisotropy factor, $\mathbf{k}=\{k_1,k_2\}$ is a spatial wave vector with absolute value $k=\sqrt{k_1^2+k_2^2}$, and f is the frequency of the Laplace transformation. The corresponding Fourier–Laplace image of polarization response is $\tilde{p}(\mathbf{k},z,f)=1/2\pi\int_0^\infty dt\int_{-\infty}^{\infty}dx\int_{-\infty}^{\infty}dy\,\exp(ik_1x+ik_2y-ft)p(x,y,z,t)$.

Under the condition $h\to\infty$, the initial and boundary conditions for perturbation $p(x,y,z,t)$ are $p(\mathbf{r},t\le 0)=0$ and $\partial p/\partial z|_{z=0}=0$. We derived the linearized solution of Eq. (4) in the form

$$\tilde{p}(\mathbf{k},z,f)=\varepsilon_{33}^{b}\varepsilon_0\tilde{V}_e(k,f)\frac{(k^2/\gamma_b^2-s_1^2)(k^2/\gamma_b^2-s_2^2)}{s_1s_2(s_1^2-s_2^2)}[s_2\exp(-s_1z)-s_1\exp(-s_2z)]. \tag{6}$$

The eigenvalues $s_{1,2}(k,f)$ are positive roots of the biquadratic equation $(s^2-k^2/\gamma_b^2)(\alpha_R+\Gamma f+\xi k^2-\xi s^2)=-s^2/(\varepsilon_0\varepsilon_{33}^{b})$, namely,

$$s_{1,2}^2(k,f)=\left(\frac{1+[k^2\xi(\gamma_b^{-2}+1)+\alpha_R+\Gamma f]\varepsilon_0\varepsilon_{33}^{b}}{2\varepsilon_0\varepsilon_{33}^{b}\xi}\pm\frac{1}{2\varepsilon_0\varepsilon_{33}^{b}\xi}\sqrt{\{1+[k^2\xi(\gamma_b^{-2}+1)+\alpha_R+\Gamma f]\varepsilon_0\varepsilon_{33}^{b}\}^2-4(\varepsilon_{33}^{b}\varepsilon_0)^2\xi(k^2\xi+\alpha_R+\Gamma f)k^2/\gamma_b^2}\right). \tag{7}$$

Note that the depolarization field (terms proportional to ε_0) and correlation effects (terms proportional to ξ) determine the spectrum $s_{1,2}(k,f)$.

The approximate closed form expression for the linearized solution has the form

$$p(\mathbf{r},f)\approx-\int_0^{\infty}\frac{k^2}{\gamma_b}dk\cdot J_0(k\rho)\tilde{V}_e(k,f)\frac{[s_2\exp(-s_1z)-s_1\exp(-s_2z)]}{\sqrt{\xi(\xi k^2+\alpha_R+\Gamma f)}(s_1^2-s_2^2)}. \tag{8}$$

Here, J_0 is the zero order Bessel function.

For typical relaxor ferroelectric parameters and $\varepsilon_{33}^{b}\leq 10$, the inequality $2\varepsilon_0\varepsilon_{33}^{b}|\alpha|\ll 1$ is valid, and so the integral in Eq. (8) reduces to the approximate explicit form

$$p(\rho,z=0,f)\approx\frac{\sqrt{\varepsilon_{11}\varepsilon_0/(\alpha_R+\Gamma f)}d^2\cdot V(f)}{[d\sqrt{\xi/(\alpha_R+\Gamma f)}+d^2+\rho^2]\sqrt{d^2+\rho^2}}. \tag{9}$$

The Laplace original is

$$p(\rho,z=0,t)\approx\frac{d^2\sqrt{\varepsilon_{11}\varepsilon_0}}{\sqrt{\Gamma}(d^2+\rho^2)^{3/2}}\int_0^t dt'\,V(t-t')f(t'),$$

$$f(t)=\exp\left(-\frac{\alpha_R}{\Gamma}t\right)\left\{\frac{1}{\sqrt{\pi t}}-\frac{d}{(d^2+\rho^2)}\sqrt{\frac{\xi}{\Gamma}}\exp\left[\frac{d^2}{(d^2+\rho^2)^2}\frac{\xi}{\Gamma}t\right]\mathrm{erfc}\left[\frac{d}{(d^2+\rho^2)}\sqrt{\frac{\xi}{\Gamma}t}\right]\right\}. \tag{10}$$

Further analytical results were obtained for the case of a rectanglelike temporal dependence of the voltage pulse, $V_a(t)=V[\theta(t)-\theta(t-t_0)]$, with pulse duration t_0, namely

$$p(\rho,z=0,t,\tau)\approx P_0(\rho)\times\left\{\theta(t)F\left[\frac{1}{\tau},\frac{d^2}{(d^2+\rho^2)^2}\frac{\xi}{\Gamma},t\right]-\theta(t-t_0)F\left[\frac{1}{\tau},\frac{d^2}{(d^2+\rho^2)^2}\frac{\xi}{\Gamma},t-t_0\right]\right\}, \tag{11}$$

where the amplitude, $P_0(\rho)=Vd\sqrt{\varepsilon_{11}\varepsilon_0}/\sqrt{\xi}\sqrt{d^2+\rho^2}$, is radially dependent, and the relaxation time, $\tau=\Gamma/\alpha_R$, is introduced at $\alpha_R>0$. The function F is given by

$$F(A,B,t)=\frac{\sqrt{B}\{1-\exp[(B-A)t]\mathrm{erfc}(\sqrt{Bt})\}-\sqrt{A}\,\mathrm{erf}(\sqrt{At})}{B-A}\approx\approx\frac{1}{\sqrt{A}+\sqrt{B}}-\frac{\exp(-At)}{B-A}\left(\frac{\sqrt{B}}{\sqrt{1+Bt}}-\frac{\sqrt{A}}{\sqrt{1+At}}\right)\sim\frac{1}{\sqrt{B}}-\frac{\exp(-At)}{\sqrt{B}}. \tag{12}$$

The temporal behavior of polarization as a function of bias pulse magnitude and time is shown in Fig. 6. For the case $A\ll B$, the response decreases with time as $t^{-3/2}$ [at least for $(t-t_0)\sim 1/B\ll 1/A$, Figs. 6(b) and 6(d)], while for the case $A>B$ the response decreases with time as $\exp(-At)$ [which is valid for $(t-t_0)>1/A$]. Close examination of the curves in Fig. 6 illustrates that under certain conditions, the almost linear regions in log-linear coordinates (corresponding to an experimentally observed logarithmic law) can be found over 1–2 decades in time. However, the full lifetime of bias induced state varies by no more than ~1 order of magnitude, well below that observed experimentally. This analysis illustrates that the spatial dispersion in a PFM experiment can broaden the relaxation time distribution and renormalize the relaxation time coefficient as Γ/α_R, but, generally by no more than one order of magnitude.

2. Intrinsic relaxation behavior

a. Nonlinear relaxation with single relaxation time. To get insight into intrinsic relaxation behavior in a uniform field, we consider a collection of individual systems with defined Debye relaxation times. The individual system without gradient effects and applied bias ($V=0$), can be described by the

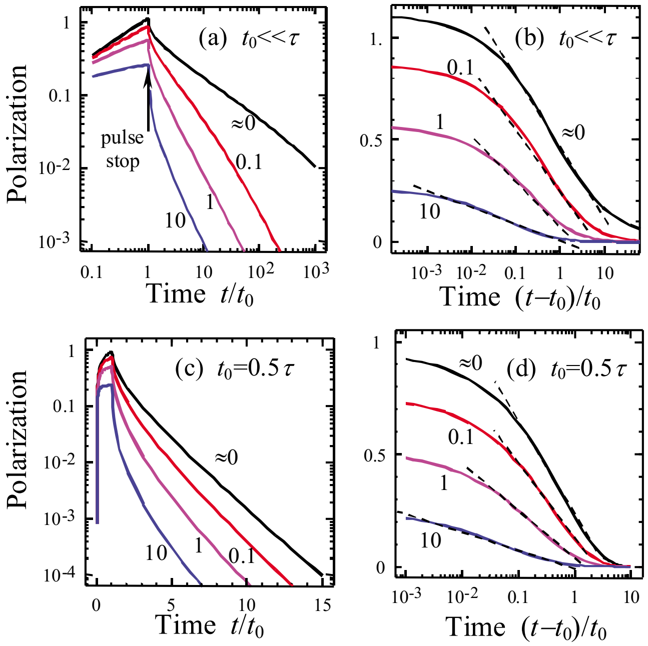

FIG. 6. (Color online) Normalized polarization response vs time for different values of parameters, t_0=0, 0.1, 1, 10 (values near the curves), and $t_0 \ll \tau$ [log-log scale (a) and log-linear scale (b)], $t_0=0.5\tau$ [linear-log scale (c) and log-linear scale (d)] at fixed bias pulse durability. Dashed lines in (b, d) indicate the linear (log) regions.

equation $\Gamma dP/dt+\alpha_R P+\beta P^3=0$, which follows a well-known nonlinear relaxation solution for positive coefficient β

$$P=\frac{P_0\zeta}{\sqrt{\beta P_0^2(1-e\zeta^2)/\alpha_R+1}}, \tag{13}$$

where P_0 is the initial value and $\zeta=\exp(-\alpha_R t/\Gamma)$.

For positive α_R (ergodic state) one obtains from Eq. (13) that the individual element follows almost exponential dynamics $P\approx P_0\exp(-t/\tau)$ at $t\gg\tau/2$, with the relaxation time $\tau=\Gamma/\alpha_R$ [compare dashed and dotted curves in Fig. 7(a)].

For negative α_R (nonergodic state), one obtains from Eq. (13) that $P\approx P_S/\sqrt{(2t/\tau)+(P_S^2/P_0^2)}$ under the condition $P_S^2 \ll P_0^2$ and times $0<t\ll\tau/2$, while $P\approx P_S$ at times $t\gg\tau/2$, where $\tau=-\Gamma/\alpha_R$ and $P_S^2=|\alpha_R|/\beta$ [see solid curves in Fig. 7(a)]. Overall, the ferroelectric cubic nonlinearity results in a significant deviation of the relaxation law from exponential for $P_S^2<P_0^2$, leading to an almost logarithmic behavior. However, the corresponding lifetime decreases for large deviations from initial state, contrary to our experimental observations. Furthermore, the effects of spatial dispersion and ferroelectric nonlinearity will partially compensate each other.

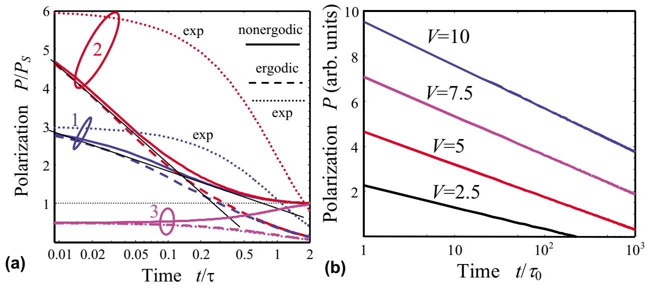

FIG. 7. (Color online) (a) Polarization relaxation at different initial values $P_0=3P_S$ (curves 1), $P_0=6P_S$ (curves 2), and $P_0=0.5P_S$ (curves 3) for nonergodic (solid), ergodic (dashed), and exponential (dotted) cases. (b) Polarization relaxation calculated from Eq. (17) at different initial voltages V (values near the curves) and V_m=5 with parameter a_f=0.25.

b. Linear relaxation with relaxation time spectrum. To rationalize experimental observations, we consider the presence of a broad relaxation time distribution in the nanoscale volume of material below the probe. We assume the relaxation time depends on the local potential energy, E, in accordance with the Vogel–Fulcher relationship, namely $\tau(E)=\tau_0\exp[E/(T-T_f)]$, and neglect the ferroelectric nonlinearity considered in the previous Sec. III C 1. Assuming the distribution of relaxation times can be described by a normalized distribution function, $g(\tau)$, the average response is $\langle P\rangle=P_0\int_0^\infty d\tau\cdot g(\tau)\exp(-t/\tau)$ at times $t>t_0$. The relaxation law in terms of a distribution function of energies $G(E)\equiv\tau(E)g[\tau(E)]/(T-T_f)$ is

$$\langle P\rangle=P_0\int_{E_{\min}}^{E_{\max}} dEG(E)\exp\left(-\frac{t}{\tau(E)}\right), \tag{14}$$

since $d\tau/dE=\tau(E)/(T-T_f)$. The observed logarithmic relaxation is consistent with a uniform energy normalized distribution function, $G(E)\approx(E_{\max}-E_{\min})^{-1}$ (Ref. 22) in the interval $E\in(E_{\min},E_{\max})$. This yields

$$\langle P\rangle=\frac{P_0(T-T_f)}{E_{\max}-E_{\min}}Ei\left[-\frac{t}{\tau_0}\exp\left(\frac{-E_{\min}}{T-T_f}\right)\right] - Ei\left[-\frac{t}{\tau_0}\exp\left(\frac{-E_{\max}}{T-T_f}\right)\right], \tag{15}$$

where $Ei(z)=-\int_{-z}^{\infty}dy\exp(-y)/y$ is an exponential integral function, for which $-Ei(-z\to-\infty)\to\exp(-z)/z$ and $Ei(-z\to0)\to\gamma+\ln z-z$, where the Euler constant $\gamma=0.577$.[37] At intermediate times, $\tau_{\min}\ll t\ll\tau_{\max}$ $\{\tau_{\min,\max}=\tau_0\exp[E_{\min,\max}/(T-T_f)]\}$, Eq. (15) can be simplified as

$$\langle P\rangle\approx P_0\left[1-\frac{T-T_f}{E_{\max}}\gamma-\frac{T-T_f}{E_{\max}}\ln\left(\frac{t}{\tau_0}\right)\right]. \tag{16}$$

Equation (16) predicts the logarithmic decay of polarization with the slope and intercept determined by the Vogel–Fulcher temperature, T_f, and the upper cut-off of the activation energy spectrum, $E_{\max}$. Experimental observations suggest that $E_{\max}$ is a function of bias amplitude, V, i.e., an increase in the bias magnitude activates the slower, higher-energy degrees of freedom in the material. Keeping in mind that $P_0\sim V$, in accordance with comments to Eq. (11) and assuming that $E_{\max}=E_{\max}^0(1+V/V_m)$, where V_m is characteristic bias, we obtained from Eq. (16) that

$$\langle P\rangle\sim V\left(1-\frac{a_f\gamma}{1+V/V_m}\right)-\frac{a_f V}{1+V/V_m}\ln\left(\frac{t}{\tau_0}\right), \tag{17}$$

with the parameter $a_f=(T-T_f)/E_{\max}$. Note that the functional form of Eq. (17) is close to the experimentally observed relaxation law given by Eq. (1a). The overall behavior is shown in Fig. 7 and is close to that observed experimentally.

D. PFS

The goal of spatially-resolved spectroscopy of relaxor materials is to obtain insight into the spatial distribution of relaxation behavior and its relationship with existing domain structures, surface topography, and structural and morphological defects. The time-resolved studies reported above provide insight into local relaxation behavior at a single point. However, the detailed studies of relaxation behavior over a dense spatial grid required to map spatial variability of relaxation behavior involve extremely large times, rendering these measurements challenging due to limitations of the microscope platform (thermal drift, data acquisition times).[22] At the same time, single point spectroscopy measurements suggest universality between voltage and time dynamics (see below). The fact that responses are linear in bias and logarithmic in time suggests that voltage spectroscopy allows a more rapid and efficient approach to probe local relaxation behavior. In this section, we present the results of voltage spectroscopy on relaxor surfaces. Section III D 1 establishes the relationship between voltage and time spectra. Section III D 2 illustrates the hysteresis loops for different PMN-PT compositions. Finally, Section III D 3 describes relaxation gap mapping of PMN-PT crystal surfaces.

1. Voltage versus time spectroscopy

To establish the relationship between voltage and time spectroscopy, we assume that the bias- and voltage dynamics follows Eqs. (1) and (2) as $\Delta PR(t)=a(V,\tau)-b\log t$, where $a(V,\tau)=(\alpha+\beta\log\tau)kV$ for $V>V_{\text{crit}}$ (bias-induced state) and 0 for $V<V_{\text{crit}}$ (no bias-induced state or short-lived state). In other words, we assume that at $V>V_{\text{crit}}$ relaxation depends only on the amount of induced polarization with universal relaxation rate, b, independent of writing process conditions. In a PFM spectroscopy experiment, a series of rectangular pulses of length τ_p spaced at τ_o (typically, $\tau_p\sim\tau_o$ and is of the order of 1–10 ms) is applied to the tip. The envelope of the wave form is a triangular wave with amplitude $V_{\max}$ (bias window) (Fig. 8). Note that in spatially resolved experiments the loops are acquired on a dense mesh, i.e., the pixel spacing is smaller than the characteristic size of the electric field produced by the probe. Hence, we are in the "quasistationary" state where we have created a "poled" state everywhere. In other words, we assume that each pixel prior to measurement cycle has experienced multiple other cycles and is in the stationary response regime.

The behavior of the hysteresis loops can be reconstructed from time dynamics as follows. If the life time of bias-induced state is less than the point measurement time, τ_p, or the tip bias V is less than V_{crit}, the response is constant. For larger voltages, a bias-induced state is created. From $a(V,\tau)=(\alpha+\beta\log\tau)kV$ we obtain $da/dt=\beta kV/t$. Hence, for a linear ramp, $V=ct$, we get $da/dt=\beta kc$ for $V>V_{\text{crit}}$ and hence the hysteresis loop is linear in voltage above a critical voltage with a slope proportional to the slope in Eq. (2), i.e., the bias-dependence of the decay constant in the tip-induced state. The total amount of switched polarization is $a(V,\tau)=(\alpha+\beta\log\tau_0)kV_{\max}$. On decreasing the bias, the polarization relaxes approximately logarithmically as $\Delta PR(t)=a_{\max}-b\log(V/c)$. The relaxation will be observable if the state induced by the maximal tip bias is stable (changes by less than ~3%) on the time scale of the experiment. This difference between a linear increase and log decay results in the hysteresis loop having a characteristically "rhomboid" shape. The nucleation biases (inflection points) are determined by the lifetime of the tip bias-induced state for both polarities. Note that the built-in fields affects both positive and negative nucleation biases (PNB and NNB) differently, as discussed below. The electrostatic fields will shift the hysteresis loop, similar to imprint in conventional ferroelectrics. Hence, PNB+NNB allow mapping built-in fields. At the same time, PNB-NNB determines the stability of tip-induced state on the time of experiment, and will further be referred as the stability gap.

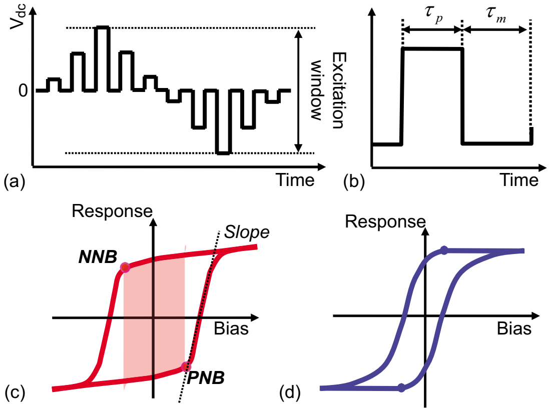

FIG. 8. (Color online) (a) Pulse sequence during the acquisition of a PFM hysteresis loop and (b) sequence of measurements at a single pulse. Schematics of a hysteresis loop for (c) ferroelectric and (d) ergodic relaxor state. In a classical ferroelectric material, the hysteresis loop shape is dominated by the *spatial dispersion* of the signal. The nucleation biases define the conditions for the nucleation of a stable domain of opposite polarity, and the slope of the loop after nucleation is determined by the bias and time dependence of the domain size. In comparison, in a relaxor ferroelectric, the hysteresis loop is dominated by the *time dispersion* of the signal, and the nucleation bias corresponds to a bias at which the lifetime of the bias-induced state becomes larger than the measurement time. The slope after nucleation is determined by the bias-dependence of the lifetime. Finally, for PNB > NNB, the bias-induced state is stable, whereas for PNB < NNB, relaxation is unstable.

The key observation in this section is that hysteresis loop formation in relaxor ferroelectrics is kinetically limited and local and is only weakly sensitive to the spatial dispersion effect. Hence, it is controlled by local properties (e.g., defined as the local relaxation time spectrum). In comparison, in classical ferroelectrics, the hysteresis loop formation is defined by nonlocal domain wall dynamics, i.e., purely by the spatial dispersion of the polarization dynamics.

2. SS-PFM

The SS-PFM maps and representative hysteresis loops from selected locations for PMN-10%PT, 32%PT, and 35%PT are shown in Fig. 9. In all cases, 2D SS-PFM maps exhibit clearly visible spatially resolved features, suggesting that the spatial variability of ferroelectric behavior is larger than the pixel spacing (dense regime). The SS-PFM maps for PMN-10%PT were recorded using a 1 V, 640 kHz ac-bias and 39.06 ms writing pulses, τ_p, followed by a 39.06 ms OFF

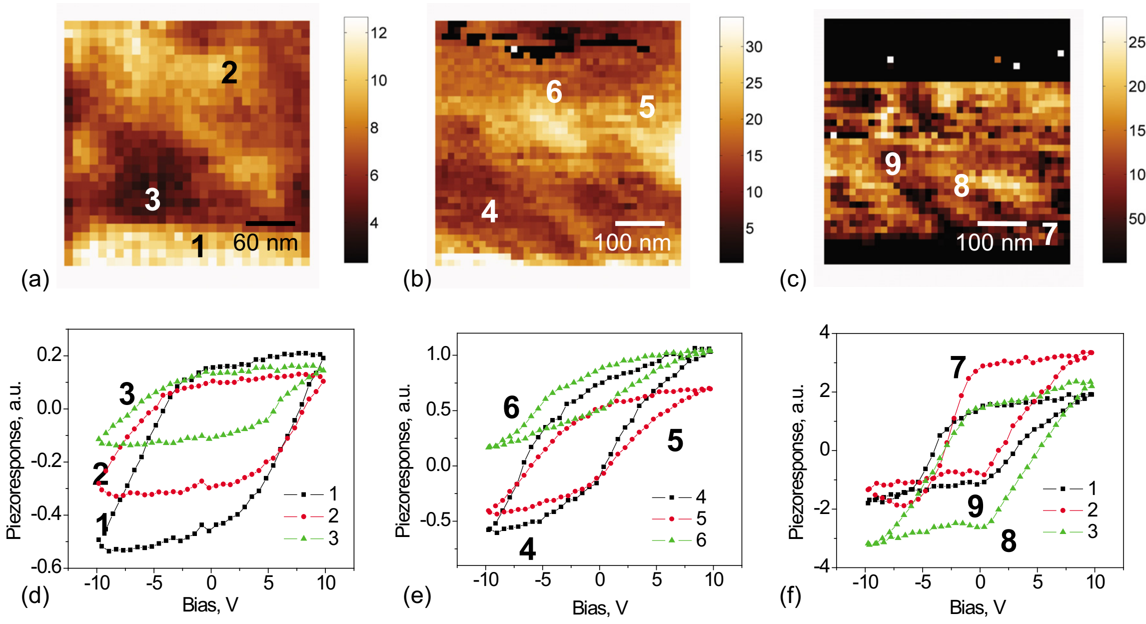

FIG. 9. (Color online) Hysteresis loops in PMN$-x$PT as a function of composition. Shown are (a, b, c) work of switching maps [in the $(-10, 10 \text{ V})$ bias window] and (d, e, f) selected hysteresis loops for (c, d) 10%PT, (b, e) 32%PT, and (e, f) 35%PT.

state, τ_o, during which time the response was recorded for 15 ms following a 15 ms delay. For 32%PT and 35%PT, the writing pulse was 110 ms, the OFF state was 47 ms, the response was recorded for 15 ms following a 15 ms delay, and the data was recorded at 5 V ac, 1.47 MHz and 1 V ac, 680 kHz, respectively. In general, in order to measure loops on 32%PT and 35%PT, a longer writing time, τ_p, was required compared to 10%PT. In PMN-10%PT, the loop shape was qualitatively the same with longer writing times and the nucleation biases remained larger than for the other compositions. The results were not very sensitive to experimental conditions [such as tips and ac voltage amplitudes and measurement frequency (away from resonances)].

The hysteresis loops for PMN-10%PT are shown in Fig. 9(d). The loops have a characteristic "diamond" shape with relatively constant response for small biases and linear increase in the response for large bias. This behavior agrees with that predicted from the observed relaxation behavior. The shape of the loops is relatively weakly position dependent, and the observed nucleation bias corresponds to the formation of a slowly (on the time scale of the measurement) relaxing polar state, as will be analyzed below.

In PMN-35%PT [Fig. 9(f)], the hysteresis loops have well-defined "ferroelectric" shape with clear nucleation biases and abrupt onset of nucleation. The corresponding nucleation bias is typically small, on the order of 0.5–2 V, and weakly position dependent. The hysteresis loops are often saturated (i.e., for high enough voltages forward and reverse branches coincide). In several locations, the formation of characteristic "noses" are observed, consistent with the presence of movable domain wall in the vicinity of the probe.[38,39] The overall behavior agrees with that expected for highly disordered ferroelectrics where a high density of random field and random bond defects allows for lower nucleation biases ~1 V (as compared to, e.g., 30 V for $LiNbO_3$ single crystals and ~5–10 V for lead zirconate titanate ferroelectric thin films) and due to proximity to T_C.

Finally, the hysteresis loops for 32%PT [Fig. 9(e)] illustrate an intermediate shape between the PMN-10%PT and PMN-35%PT cases. After nucleation, the loop shape has profound curvature, possibly due to the stronger ferroelectric nonlinearity induced by the ferroelectric phase. Similarly, the switchable component of the bias-induced polar state relaxes much faster. We ascribe this behavior to the simultaneous presence of a switchable polarization component and a nonswitchable frozen polarization.

3. Stability gap mapping

The SS-PFM maps allow the stability of bias induced states (the "stability gap") to be mapped as the lifetime exceeding the experimental time for the applied 10 V bias. Shown in Figs. 10(a)–10(d) are mixed PFM, switchable polarization, stability gap, and built-in field maps for PMN-10%PT. The image shows large scale features of ~100 nm size, indicative of the presence of mesoscopic range disorder in the material. Note that all three maps are generally uncorrelated, indicative of the veracity of the measurements. The corresponding histograms of PNB and NNB and PNB-NNB (their difference) are shown in Figs. 10(e) and 10(f). Note that a significant fraction of the sample surface has a negative PNB-NNB. This shows that the bias-induced polar state is unstable as expected for the ergodic relaxor phase.

In comparison, mixed PFM and SS-PFM maps for PMN-32%PT are shown in Fig. 11. In this case, stability gap, switchable polarization, and built-in field maps show clear contrast correlated with the remnant ferroelectric domains. Note that a larger switchable polarization corresponds to a smaller stability gap. This is anticipated, since the driving force for switching is proportional to polarization, P. Also, there are no regions with zero stability gap, i.e., the bias-

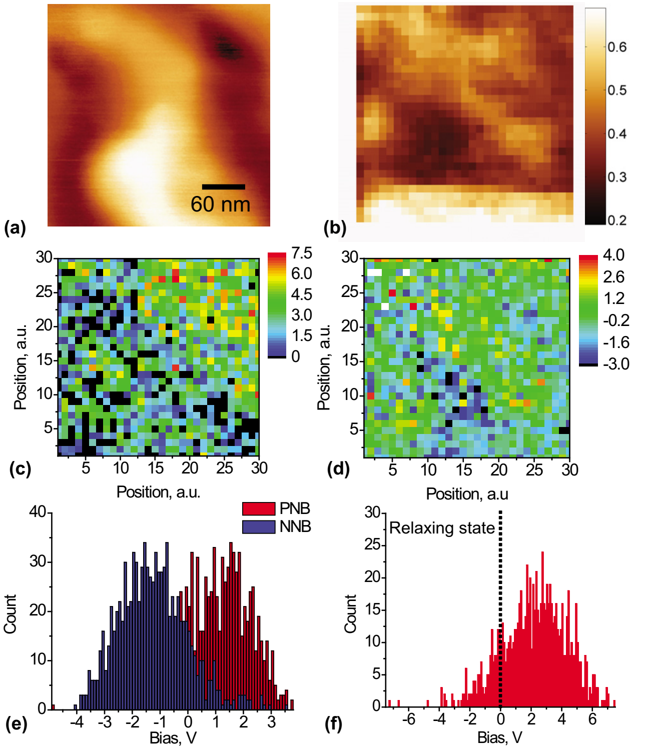

FIG. 10. (Color online) Switching spectroscopy mapping of PMN-10%PT. (a) Mixed PFM signal, (b) switchable polarization, (c) stability map [PNB-NNB], and (d) built-in field [PNB+NNB] map. Histograms of (e) PNB and NNB and (f) PNB-NNB.

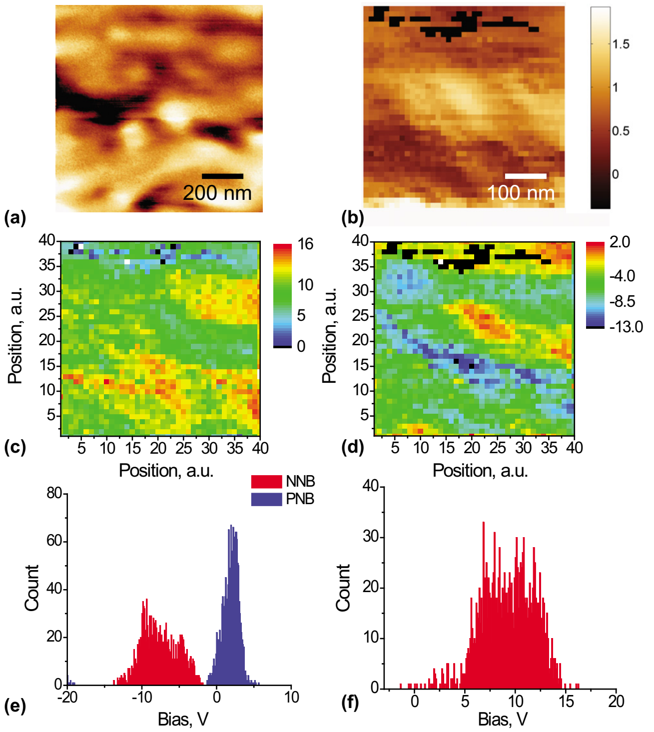

FIG. 11. (Color online) Switching spectroscopy mapping of PMN-32%PT. (a) Mixed PFM signal, (b) switchable polarization, (c) stability map [PNB-NNB], and (d) built-in field [PNB+NNB] map. Histograms of (e) PNB and NNB and (f) PNB-NNB. Panel b was measured from the center of (a). Panels (c) and (d) have the same scale as (b).

induced states are stable. This behavior is further illustrated in the histograms in Figs. 11(e) and 11(f). Here, the PNB and NNB are well separated, and PNB-NNB is always positive in contrast to PMN-10%PT. This is because the PMN-32%PT is in a ferroelectric state and the poled state induced by large enough bias field is stable. A field of opposite polarity is required to switch the polarization.

IV. SUMMARY

Domain structures and time- and bias-controlled local polarization dynamics in the PMN−xPT family of relaxor ferroelectrics are studied using PFM and PFS. The PFM imaging indicates the presence of labyrinthine domain structures even in ergodic PMN-10%PT compositions, indicative of a noncubic symmetry at least in the surface layer. In PMN-35%PT, ferroelectric domains with high wall roughness are observed, whereas PMN-32%PT demonstrates the coexistence of ferroelectric and labyrinthine domains. The comparison of vertical and lateral PFM suggests that the observed in-plane contrast can be ascribed purely to cross-talk between vertical and lateral signals, and no evidence for in-plane domains is obtained.

The dependence of relaxation behavior on the pulse amplitude and time was found to follow a universal logarithmic behavior with a nearly constant slope. This behavior is indicative of the progressive population of high energy slow relaxation states, as opposed to the linear relaxation in the presence of a broad relaxation time spectrum. The contribution of ferroelectric nonlinearity and spatial dispersion of the tip field to the relaxation is analyzed in detail, and the effects of spatial dispersion are shown to be relatively small. Hence, PFM-based relaxation experiments provide information similar to that in a uniform field.

The relationship between relaxation and hysteresis loop formation is analyzed in detail. It is shown that local hysteresis loops in relaxors are fundamentally different form those in ferroelectrics. In relaxors (PMN-10%PT), the local loops are kinetically limited, while in "normal" ferroelectrics (PMN-32%PT and PMN-35%PT) the loops seem to be dominated by the spatial dispersion of the polarization only. Finally, switching spectroscopy mapping of relaxor and ferroelectric PMN-PT compositions is performed, and the mapping of built-in fields and the stability gap is demonstrated.

ACKNOWLEDGMENTS

This research is supported by the Center for Nanoscale Materials Sciences (B.J.R., S.J., S.V.K.) at the Oak Ridge National Laboratory, Division of Scientific User Facilities, Office of Basic Energy Sciences, U.S. Department of Energy and was part of a CNMS User Program (CNMS2007-085). The research is also sponsored by the Ministry of Science and Education of Ukraine and the National Science Foundation through the Materials World Network, Grant No. DMR-0908718(A.N.M. and S.V.S.). D.A.K. and A.L.K. are grateful to Portuguese Foundation for Science and Technology (FCT) (PhD fellowship grant SFTH/BD/22391/2005 and project PTDC/FIS/81442/2006). The work is further supported (A.A.B., Z.G.Y.) by the Office of Naval Research (Grant No. N00014-06-1-0166). B.J.R. also acknowledges the support of UCD Research. We thank Nanotec Electronica for providing the free software WSxM, which has been used to process images in Figs. 1 and 2 (http://www.nanotec.es).

[1] W. Kleemann, J. Mater. Sci. **41**, 129 (2006).
[2] A. A. Bokov and Z.-G. Ye, J. Mater. Sci. **41**, 31 (2006).
[3] H. Yu, V. Gopalan, J. Sindel, and C. A. Randall, J. Appl. Phys. **89**, 561 (2001).
[4] P. Lehnen, W. Kleemann, T. Woike, and R. Pankrath, Phys. Rev. B **64**, 224109 (2001).
[5] M. Abplanalp, D. Barošová, P. Bridenbaugh, J. Erhart, J. Fousek, P. Günter, J. Nosek, and M. Šulc, Solid State Commun. **119**, 7 (2001).
[6] S. B. Vakhrushev, A. A. Naberezhnov, B. Dkhil, J.-M. Kiat, V. Shvartsman, A. Kholkin, B. Dorner, and A. Ivanov, *Fundamental Physics of Ferroelectrics 2003*, AIP Conf. Proc. No. 67 (AIP, New York, 2003), p. 74.
[7] F. Bai, J.-F. Li, and D. Viehland, Appl. Phys. Lett. **85**, 2313 (2004).
[8] V. V. Shvartsman and A. L. Kholkin, Phys. Rev. B **69**, 014102 (2004).
[9] A. N. Salak, V. V. Shvartsman, M. P. Seabra, A. L. Kholkin, and V. M. Ferreira, J. Phys.: Condens. Matter **16**, 2785 (2004).
[10] H. R. Zeng, H. F. Yu, S. X. Hui, G. R. Li, H. S. Luo, and Q. R. Yin, J. Cryst. Growth **267**, 194 (2004).
[11] V. V. Shvartsman, A. L. Kholkin, A. Orlova, D. Kiselev, A. A. Bogomolov, and A. Sternberg, Appl. Phys. Lett. **86**, 202907 (2005).
[12] V. V. Shvartsman and A. L. Kholkin, J. Appl. Phys. **101**, 064108 (2007).
[13] M. Molotskii, J. Appl. Phys. **93**, 6234 (2003).
[14] A. L. Kholkin *et al.*, (unpublished).
[15] Z.-G. Ye, Y. Bing, J. Gao, A. A. Bokov, P. Stephens, B. Noheda, and G. Shirane, Phys. Rev. B **67**, 104104 (2003).
[16] A. K. Singh, D. Pandey, and O. Zaharko, Phys. Rev. B **74**, 024101 (2006).
[17] D. Zekria, V. A. Shuvaeva, and A. M. Glazer, J. Phys.: Condens. Matter **17**, 1593 (2005).
[18] S. Jesse, A. P. Baddorf, and S. V. Kalinin, Appl. Phys. Lett. **88**, 062908 (2006).
[19] V. V. Shvartsman, A. L. Kholkin, M. Tyunina, and J. Levoska, Appl. Phys. Lett. **86**, 222907 (2005).
[20] B. J. Rodriguez, S. Jesse, J. Kim, S. Ducharme, and S. V. Kalinin, Appl. Phys. Lett. **92**, 232903 (2008).
[21] S. V. Kalinin, B. J. Rodriguez, S. Jesse, A. N. Morozovska, A. A. Bokov, and Z.-G. Ye, Appl. Phys. Lett. **95**, 142902 (2009).
[22] S. V. Kalinin, B. J. Rodriguez, J. D. Budai, S. Jesse, A. N. Morozovska, A. A. Bokov, and Z.-G. Ye, Phys. Rev. B **81**, 064107 (2010).
[23] B. J. Rodriguez, S. Jesse, A. A. Bokov, Z.-G. Ye, and S. V. Kalinin, Appl. Phys. Lett. **95**, 092904 (2009).
[24] R. C. O'Handley, *Modern Magnetic Materials: Principles and Applications* (Wiley-Interscience, New York, 2000).
[25] I. K. Bdikin, V. V. Shvartsman, and A. L. Kholkin, Appl. Phys. Lett. **83**, 4232 (2003).
[26] D. A. Kiselev, I. K. Bdikin, E. K. Selezneva, K. Bormanis, A. Sternberg, and A. L. Kholkin, J. Phys. D: Appl. Phys. **40**, 7109 (2007).
[27] B. Noheda, D. E. Cox, G. Shirane, J. Gao, and Z.-G. Ye, Phys. Rev. B **66**, 054104 (2002); Z.-G. Ye, B. Noheda, M. Dong, D. Cox, and G. Shirane, *ibid.* **64**, 184114 (2001).
[28] M. Abplanalp, Ph.D. thesis, ETHZ, 2001.
[29] A. N. Morozovska, E. A. Eliseev, S. L. Bravina, and S. V. Kalinin, Phys. Rev. B **75**, 174109 (2007).
[30] J. Guyonnet, H. Béa, F. Guy, S. Gariglio, S. Fusil, K. Bouzehouane, J.-M. Triscone, and P. Paruch, Appl. Phys. Lett. **95**, 132902 (2009).
[31] A. A. Bokov and Z. G. Ye, J. Appl. Phys. **95**, 6347 (2004).
[32] D. Andelman and J. F. Joanny, Phys. Rev. B **32**, 4818 (1985).
[33] W. Kleemann, Int. J. Mod. Phys. B **7**, 2469 (1993).
[34] A. K. Tagantsev and G. Gerra, J. Appl. Phys. **100**, 051607 (2006).
[35] C. H. Woo and Y. Zheng, Appl. Phys. A **91**, 59 (2007).
[36] A. N. Morozovska, S. V. Svechnikov, E. A. Eliseev, S. Jesse, B. J. Rodriguez, and S. V. Kalinin, J. Appl. Phys. **102**, 114108 (2007).
[37] I. S. Gradshteyn and I. M. Ryzhik, in *Table of Integrals, Series, and Products*, 5th ed., edited by A. Jeffrey (Academic, New York, 1994).
[38] A. K. Tagantsev, P. Muralt, and J. Fousek, *Ferroelectric Thin Films XII*, MRS Symposia Proceedings No. 784 (Materials Research Society, Pittsburgh, 2004), p. C10.6.
[39] G. Le Rhun, I. Vrejoiu, L. Pintilie, D. Hesse, M. Alexe, and U. Gösele, Nanotechnology **17**, 3154 (2006).
[40] S. V. Kalinin, A. N. Morozovska, L. Q. Chen, and B. J. Rodriguez, Rep. Prog. Phys. **73**, 056502 (2010).